Technical Article

Challenges in the Synthesis of NFC Transponders

***Abstract* — The near field communication (NFC) technology with several applications like contactless payment or access control has become common in our daily life, especially due to its simplicity and intuitive operation. Nevertheless, the way from an application idea to the final product is anything but easy. Beside the facts that e.g. some geometrical limitations for the antenna have to be fulfilled – which naturally also influence the electromagnetic behavior of the specific antenna – a rather large number of standard conformity tests have to be executed and passed with prototypes to finally be able to bring the device onto the market. In the following an approach is presented which allows the incorporation of technical specifications of standardization tests for NFC devices already in the design phase of the NFC antenna. This approach should help to dramatically reduce the number of redesigns in the product development of specific NFC devices and consequently also reduce the number of time consuming and expensive test measurements. The approach is based on a numerical optimization technique assisted by a partial element equivalent circuit (PEEC) method which allows the synthesis of an NFC antenna and the attached matching circuit.**

I. Introduction

NFC is a rather new technology which is based on the radio frequency identification (RFID) technology. NFC, more specifically the NFC data exchange format (NDEF) can be seen as a kind of roof standard to the most common HF-RFID standards like the ISO/IEC 14443 [1] proximity card standard, the ISO/IEC 15693 [2] vicinity card standard or the FeliCa [3] standard. As the name already reveals the contactless communication between the communication participants is established in the near field "surrounding" them as should be depicted by the principle sketch in Fig. 1 taken form the NFC Forum Analog Technical Specification [4].

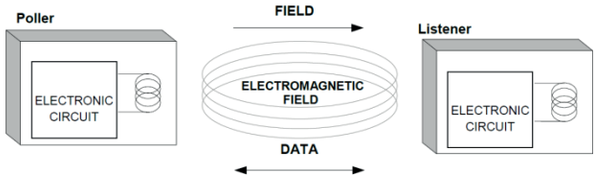

Fig. 1. NFC Poller and Listener configuration [4].

First commercial RFID applications where mainly located in the low frequency band (125 kHz, 134.2 kHz), like animal identification or electronic vehicle immobilizers in the 1980s. The antennas for such applications were rather big and expensive. Therefore, due to size and cost reduction needs, the operating frequency was increased to the high frequency band. First to 8.2 MHz and later to 13.56 MHz, where the above mentioned standards are valid. Also in the ultra-high frequency band (860 MHz - 960 MHz) RFID applications are located, but these application are typically based on the backscattering of electromagnetic waves and are not covered by NFC. A comprehensive summary of the historical development of RFID and NFC as well as the corresponding standards can be found in [5].

The role of the communication participants in RFID systems is strictly defined: a so called reader/interrogator or polling device provides by means of a loop antenna a magnetic field. This magnetic field, which for so called passive devices is also used for the powering, is modulated with the data to be transmitted to the listener/transponder. The reader is also responsible for the complete control of the communication with the RFID transponder. Such RFID transponders (e.g. smart cards, smart labels, electronic tickets, etc.) typically consist of a loop antenna, a matching circuit and an IC. Hence, from an electrical engineering point of view the system can be seen as a transformer. Due to energy efficiency reasons the system is operated in resonance. This means that the impedance of the transmitting loop of the reader is heavily influenced by the receiving loop antenna of the transponder and the dynamic impedance of the IC connected to this loop. In principle this change of the impedance is used for the communication from the transponder to the reader. The underlying communication technique is called load modulation [5].

Depending on the kind of application the IC connected to the loop has a lower or higher functionality. E.g. for payment application also a cryptographic co-processor is integrated to ensure a secure communication. Naturally the energy consumption for such a transponder is much higher than for applications with a very low security level. Hence, also the operating range is limited due to the regulations for the emitted H-field. Therefore, all aspects of power transfer, read range and communication depend on the impedance of the transmitting loop antenna and need to be considered in the antenna design [5].

Due to the fact that NFC is a roof standard for many RFID applications as mentioned before, it is obvious that the antenna design for devices compatible to the definitions in the NFC Forum is quite challenging. This is even more the case due to the fact that NFC devices can be both reader and transponder and can also change their communication mode in contrast to RFID where the role in the communication control is strictly defined. The operational modes are summarized in Fig. 2.

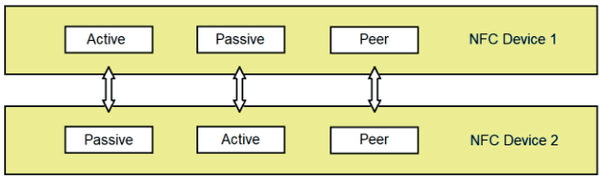

Fig. 2. Operation modes for NFC devices [6].

Beside the physical requirements also the requirements on the communication protocol are demanding but those will not be treated in this work. In the following we will concentrate only on the so called air interface which includes the loop antennas and the matching circuits to match the NFC-IC to the antenna. A very common and still well established work flow for designing loop antennas is based on analytical models which utilize equivalent circuit descriptions and system level quantities like the quality factor, minimum required H-field strengths, etc. In the references [7] - [11] a comprehensive summary of such analytical approaches can be found. A major drawback of these models is given by the fact that parasitic influences like e.g. eddy currents in conducting materials close to the antenna structure can hardly be taken into account. Additionally, typically the strong non-linear behavior of the

NFC IC's analog RF interface is also neglected. It should be noted at this point that also the standardization test equipment has a strong non-linear electric behavior as will be discussed in detail in section III. After having obtained the requirements on the antenna based on the analytical models in general the matching circuit is developed, hence from the optimization point of view this approach cannot be seen as rigorous and it is not guaranteed that the so obtained design is indeed the optimum design. Furthermore, it is hardly possible to conduct the required standardization test based on such analytical descriptions which consequently leads to a rather costly production of prototype devices and related measurements. Therefore, we propose a rigorous synthesis of the loop antenna geometry and the matching circuit taking into account NFC-IC specific quantities like the maximum current, specific standardized requirements on the H-filed in the operating volume as well as requirements on the data rates at the air interface. The synthesis is based on a PEEC aided numerical optimization approach. The big advantage applying PEEC is given by the fact that the matching circuit can be directly incorporated into the PEEC model of the antenna and solved as one system of equations.

The remainder of the article is organized as follows: Section II gives a short introduction to PEEC in general and an overview of the applied wire-based technique. In section III the considered NFC specifications are summarized. Here we concentrate on the power requirement test and the communication of the NFC device in the so called polling mode. The optimization problem is presented in section IV. Here the construction of the loop geometry, a pre-investigation on the parameter space of the optimization problem as well as the construction of the cost function and the applied optimization strategies is discussed. Section V summarizes the obtained results as well as discusses the obtained design variables. Finally in section VI a conclusion and outlook is given.

II. Applied PEEC Method

The main advantage of the PEEC method first proposed by Ruehli [12] compared e.g. to the finite element method is given by two facts: first, the air volume surrounding the conductive material does not need to be discretized and second, the resulting system of equations describing the electromagnetic behavior of the conducting structure allows a simple connection of lumped electric components. In the following a brief introduction to the PEEC method is presented.

The formulation of the time harmonic PEEC method starts from the well known Electric Field Integral Equation (EFIE):

$$\mathbf{E} = -i\omega\mathbf{A} - \nabla\varphi + \mathbf{E}_{\mathbf{ext}}, \tag{1}$$

where $\mathbf{E}$ is the electric field, $\mathbf{A}$ is the vector magnetic potential, φ is the scalar electric potential and $\mathbf{E}_{\mathbf{ext}}$ is the external electric field. With the charge conservation law $\mathbf{A}$ and φ in (1) are given by the following integral expressions [13]:

$$\mathbf{A}(\mathbf{r}) = \mu_0 \int_\Omega \mathbf{J}(\mathbf{r}')g(\mathbf{r},\mathbf{r}')\mathrm{d}\Omega', \tag{2}$$

$$\varphi(\mathbf{r}) = -\frac{1}{i\omega\varepsilon_0}\int_\Omega \nabla\cdot(\mathbf{J}(\mathbf{r}')g(\mathbf{r},\mathbf{r}'))\mathrm{d}\Omega', \tag{3}$$

where $\mathbf{J}$ is the conduction current density, $g(\mathbf{r},\mathbf{r}')$ is the Green's function, $\mathbf{r}$ is the field point and $\mathbf{r}'$ is the integration point. μ_0 and ε_0 are the permeability and the permittivity of vacuum, respectively. Ω is the conductive domain.

For linear conductive media, Ohm's law holds:

$$\mathbf{E} = \rho\mathbf{J}, \quad in\ \Omega, \tag{4}$$

where ρ is the electric resistivity.

Let's now consider that the conductive domain Ω is made by thin conductive wires (see, e.g., Fig. 3).

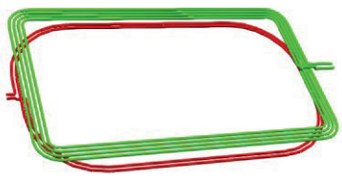

Fig. 3. Two closely coupled wire based loop antennas.

Such kind of structure can be easily represented by using stick wire elements for the discretization. Thus, a mesh made by N_e stick elements (edges) and N_n nodes is introduced. Moreover, a dual mesh made by the barycenteric subdivision of the primal one is also introduced. Edges and nodes of the primal grid are into a one-to-one relation with nodes and edges of the dual grid, respectively.

Then, the current density $\mathbf{J}$ is expanded as

$$\mathbf{J}(\mathbf{r}) = \sum_k^{N_e} j_k\, \mathbf{w}_k(\mathbf{r}), \tag{5}$$

where $\mathbf{w}_k$ is the vector shape function and j_k is the Degree of Freedom (DoF) related to the kth stick element of the mesh. The shape function $\mathbf{w}_k$, in its support (i.e. the kth stick element) is given by

$$\mathbf{w}_k(\mathbf{r}) = \frac{\mathbf{u_k}}{\mathrm{A_k}}, \tag{6}$$

where $\mathbf{u_k}$ is the unit vector along the kth stick element and $\mathrm{A_k}$ is the cross section area of the kth stick element. In the original PEEC method, both $\mathbf{J}$ and φ are considered as unknowns. Thus, it is convenient to introduce the following expansion for φ:

$$\varphi(\mathbf{r}) = \sum_k^{N_n} \phi_k\, \mathrm{p}_k(\mathbf{r}), \tag{7}$$

where $\mathrm{p_k}$ is the shape function and ϕ_k is the DoF related to the kth node of the mesh. The shape function p_k is given by

$$\mathrm{p}_k(\mathbf{r}) = \frac{\mathbf{1}}{\mathrm{l_k}}, \tag{8}$$

where $\mathrm{l_k}$ is the length of the kth dual edge related to the kth primal node of the mesh.

By using (5) and (7) in (1)-(4) and projecting the resulting equations by applying a Galerkin scheme, the following PEEC system of equations is obtained:

$$\begin{bmatrix} \mathbf{R}+i\omega\mathbf{L} & \mathbf{G} \\ \mathbf{P}\mathbf{G}^{\mathbf{T}} & -i\omega\mathbf{1} \end{bmatrix}\begin{bmatrix} \mathbf{j} \\ \boldsymbol{\phi} \end{bmatrix} = \begin{bmatrix} \mathbf{e}_{\mathbf{ext}} \\ \mathbf{0} \end{bmatrix}, \tag{9}$$

where $\mathbf{R}$, $\mathbf{L}$, and $\mathbf{P}$ are the resistance, inductance and potential PEEC matrices, $\mathbf{G}$ is the nodes-edges incidence matrix and $\mathbf{1}$ the identity matrix. $\mathbf{j}$, $\boldsymbol{\phi}$, and $\mathbf{e}_{\mathbf{ext}}$ are arrays which store the DoFs related to $\mathbf{J}$, φ, and $\mathbf{E}_{\mathbf{ext}}$, respectively. The expression of the coefficients of $\mathbf{R}$, $\mathbf{L}$, and $\mathbf{P}$ can be found in [14].

System (9) possess a circuit interpretation, indeed its first and second row can be seen as Kirchhoff's Voltages and Currents laws (KLVs and KLCs) written for each edge and node of the mesh. Therefore, (9) can be easily coupled with lumped

circuits. In such a case, (9) is modified as follows by introducing the KVLs and KCLs written for each extra lumped circuit branch and node, i.e.

$$\begin{bmatrix} \mathbf{R}+i\omega\mathbf{L} & \mathbf{G} & \mathbf{0} & \mathbf{0} \\ \mathbf{P}\mathbf{G}^{\mathbf{T}} & -i\omega\mathbf{1} & \mathbf{P}\mathbf{G}_{\mathbf{l,c}}^{T} & \mathbf{0} \\ \mathbf{0} & \mathbf{G}_{\mathbf{l,c}} & \mathbf{Z}_{l} & \mathbf{G}_{\mathbf{l,l}} \\ \mathbf{0} & \mathbf{0} & \mathbf{G}_{\mathbf{l,l}}^{\mathbf{T}} & \mathbf{0} \end{bmatrix} \begin{bmatrix} \mathbf{j_c} \\ \boldsymbol{\phi} \\ \mathbf{j_l} \\ \boldsymbol{\phi}_{\mathbf{l}} \end{bmatrix} = \begin{bmatrix} \mathbf{e_{ext}} \\ \mathbf{P}\mathbf{j_0} \\ \mathbf{e_{ext,l}} \\ \mathbf{j_{0,l}} \end{bmatrix}. \quad (10)$$

where $\mathbf{j_l}$ is the array storing the currents flowing in the lumped circuit branches, $\boldsymbol{\phi}_\mathbf{l}$ is the array storing the electric potentials of the lumped circuit nodes. $\mathbf{G_{l,c}}$ is the $N_{el} \times N_n$ incidence matrix describing the connections between the N_{el} lumped circuit branches and the nodes of the discretized devices, and $\mathbf{G_{l,l}}$ is an $N_{el} \times N_{nl}$ incidence matrix describing the connections between the N_{el} lumped circuit branches and the N_{nl} lumped circuit nodes. $\mathbf{e_{ext,l}}$ is the array storing the electric field applied to the lumped branches, $\mathbf{j_0}$ and $\mathbf{j_{0,l}}$ are arrays storing external currents injected into the circuit nodes of the mesh and lumped circuit nodes, respectively. $\mathbf{Z}_l$ is an $N_{el} \times N_{el}$ impedance matrix related to the lumped branches.

Finally, the solution of the coupled electromagnetic-circuit problem is obtained by solving (10). When the problem dimension is sufficiently small, (10) can be solved by means of a standard direct solver based, for instance, on LU decomposition. However, since **L** and **P** are fully populated matrices, the memory requirement and the computation time for solving (10) grow as $O(N^2)$ and $O(N^3)$, respectively, thus leading to possibly prohibitive computational costs. To reduce the computational burden, many works in the literature propose to exploit the low-rank property of the off-diagonal blocks of **L** and **P** by using, e.g., Hierarchical matrices coupled with Adaptive Cross Approximation [14], [15], Fast Multipole Methods [16], or other low-rank compression techniques.
In the PEEC method described above 1D stick elements are adopted for the discretization. This allows to significantly simplify the discretization of devices made by thin conductive wires (e.g. antennas). However, the adoption of this kind of elements introduces unavoidable approximations. Indeed, **J** is considered to be uniform inside each element, thus skin effects are completely neglected (unless a known current distribution is forced by using ad-hoc shape functions). Moreover, only volume electric charge density is considered. This may lead to some inaccuracies when capacitive effects between close conductive surfaces are predominant [17]. However, for many industrial high frequency application, the PEEC method with stick wires allows for a good trade-off between accuracy and computational costs especially in the pre-design phase.

III. NFC Specifications

As already pointed out in Section I NFC can be seen as roof standard for several RFID standards. Hence it is obvious that for NFC Forum standard conformity quite a large number of tests are needed. In the present work we concentrate only on the physical requirements. Within these physical requirements defined in the NFC Forum Analog Technical Specification [4] (which are constantly being adapted) two very important tests were chosen for incorporation in the design synthesis. Namely the “Poller Requirements for Power Transfer from Poller to Listener” (in the following we call this test power requirement test) and the “Poller Requirements for Modulation Poller to Listener NFC-A”. These two tests are of relevance if the device is in reader/polling mode as shown in Fig. 2. The reason for focusing only on these two tests is due to the fact that from a system level point of view they represent contrary demands on the quality factor of the NFC device’s loop antenna. From power perspectives the quality factor of the antenna should be ”as high as possible” but from the perspective of the data rate at the air interface the antenna’s quality factor has to be kept below a specific level. If the Q-factor is chosen too high the bandwidth of the resonance circuit is low and hence requirements on the timing cannot be fulfilled. In the following these two tests are explicated into more details.

A. Power-Requirement-Test

Especially for passive transponders the emitted H-field of the polling device is of extreme importance since the passive transponder is obtaining the energy for operating from the H-field provided by the polling device. On the other hand the emitted H-field must not exceed upper limits which are given by general regulations for field strengths levels (e.g. ETSI EN 300 330 [18]).
The related so called H_{min}- and H_{max}-test (two different load cases are tested representing the modulation cases of a listening device) have to be carried out by using so called NFC Forum Listener Devices (see Fig. 4(a)) which are placed at specific points in the NFC Forum Operating Volume (see Fig. 4(b)).

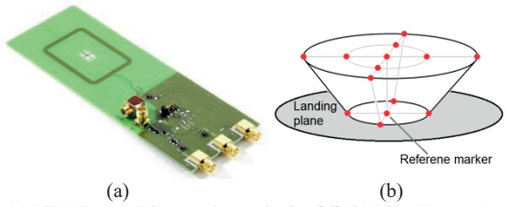

(a) (b)

Fig. 4. (a) NFC Forum Listener 3 test device [6] (b) NFC Forum Operating Volume.

Three classes of listening devices exist: the NFC Forum Listeners 1, 3 and 6. The devices differentiate from each other in terms of the size of the test antenna. E.g. the size of the Listener 1 antenna is related to the size of Class 1 antennas [1] which can be found in PICC-1 (proximity integrated circuit cards) devices. Beside the geometrical dimensions also the electric circuitry connected to the antenna is defined in the standard. For more information please refer to [4].
The power requirement compliance is defined by means of a DC-voltage measured at the variable load resistance connected after a bridge rectifier circuitry as shown in the principle sketch in Fig. 5.

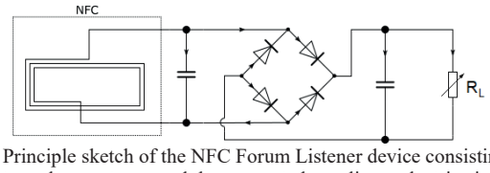

Fig. 5. Principle sketch of the NFC Forum Listener device consisting of the listener loop antenna and the connected non-linear electric circuit.

Hence, the actual compliance test described in the standard is a time domain test which has to be carried out at all 14 positions in the operating volumes with all three listeners for the two load cases. So in total a minimum of 84 (!) tests has to be carried out. Also in terms of time domain transient steady state simulations this large number of tests would result in huge computational effort and is therefore impracticable for the optimization based synthesis of the loop geometry. To overcome this problem the nonlinear electric circuitry

connected to the listener antenna has been modelled in terms of a linear equivalent load resistance where the equivalent power is dissipated as for the measured DC voltage at the variable load resistance. In a first attempt [19] the equivalent resistance values were chosen such that a resulting antenna quality factor of $Q = 30$ (which is a standard value for NFC transponders) is given. But it turned out that this is an over-simplification. Hence, we used measurement data of the DC-voltages of the listeners which were operated in the ISO/IEC 10373 test setup [20]. With those data and measured values of the corresponding equivalent H-field we were able to determine corresponding equivalent resistance values in terms of PEEC simulations of the ISO 10373 setup and consequent curve fitting with a least squares approach. A model of the test setup is shown in Fig. 6 as well as the comparison between the measured and fitted curve for the Listener 1 H_{min}-test is presented in Fig. 7. In Table I the obtained load resistance values are summarized. It should be noted that the difference between the values in Table I and the values in [21] are due to a different test setup (in [21] instead of the PCD 1 test antenna the Poller 0 antenna was used).

TABLE I. EQUIVALENT LOAD RESISTANCES FOR POWER REQUIREMENT.

Listener Device	R_{Lequiv} for H_{min}-test in Ω	R_{Lequiv} for H_{max}-test in Ω
Listener 1	400	44.5
Listener 3	378	44.5
Listener 6	205	26.5

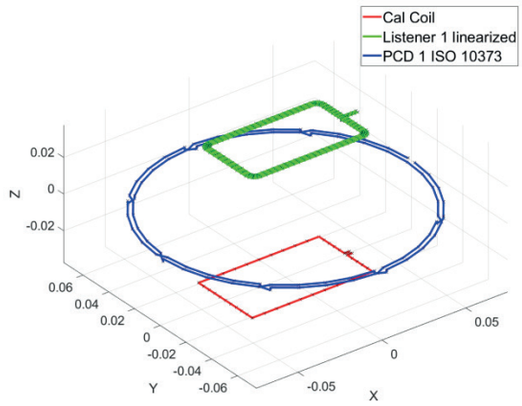

Fig. 6. PEEC model of the ISO/IEC 10373 test setup with calibration coil, PCD 1 antenna and Listener 1 coil.

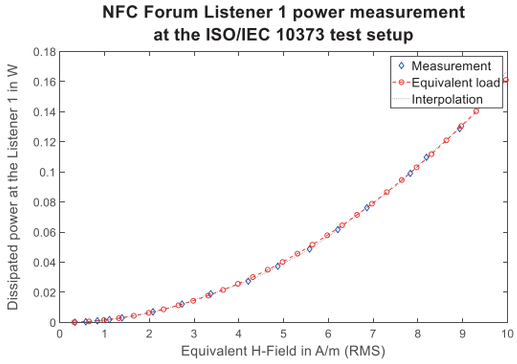

Fig. 7. Comparison of the measured and simulated power dissipated at the resistance R_{Lequiv_min} of the Listener 1.

B. Antenna quality factor and bandwidth

As already pointed out, the loop antenna quality factor is a very important system level quality which influences the two contending requirement: communication bandwidth and power transmission. A high Q-factor would be good from power perspectives but on the other hand limits the communication bandwidth. It should be noted that the quality factor is not directly stated in the analog technical specifications of the standard but we can compute upper bounds for Q from the defined signal requirements. In the present work we concentrate only on the NFC-A specifications [4].

The most rigorous way to test the digital twin of the NFC device for compliance to the standard would be a time domain simulation to obtain and compare the steady state signal shape to the definitions in the standard. But from an optimization point of view this approach is impractical due to the computational burden. Hence, the need for a frequency domain equivalence is given. Two possibilities shall be discussed in the following.

The first approach is based on a simplified second-order equivalent circuit description of the loop antenna including the matching circuit and the computation of the signal-envelope when applying a unit step function. Following the procedure proposed in [22] we obtain for the NFC-A modulation pulse shown in Fig. 8 for the shortest time interval t_4:

$$Q_{t4,A} = -\frac{t_4 . \omega_{res}}{ln(1-0.6)} \leq 40.91. \tag{11}$$

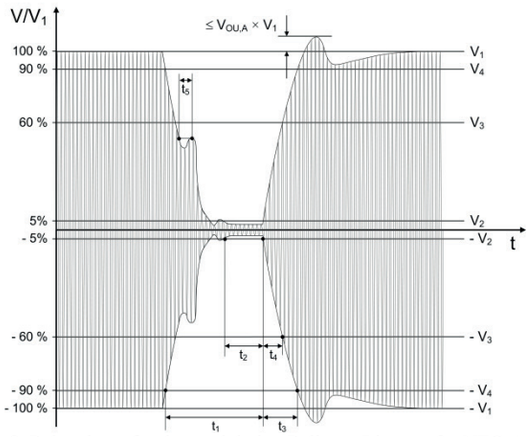

Fig. 8. Pulse shape for the modulation Poller to Listener for NFC-A [4].

The second approach is based on the time-bandwidth product of pulsed signals. For pulsed signals one is faced with the problem that a strictly time bounded signal possess an infinity spectrum in the frequency domain. Nevertheless some definitions [23] exist which enable a relationship between the time period of the signal and the covered spectrum in the frequency domain. A very general approach is given by considering the bounded energy of the signal by means of so called second moments [23]. Following [23] independent of the used approach a bound for the time-bandwidth product can be found:

$$T \cdot B \geq 0.5 \ldots 1. \tag{12}$$

With the NFC-A related modulation scheme, which is a modified Miller 100% amplitude shift keying modulation, where the detection of the falling edge and the length of the off-phase is relevant, the needed bandwidth would be:

$$B \geq \frac{1}{T} = 334.5\ kHz. \tag{13}$$

Where T is the time period between the falling edge and the subsequent rising edge of the signal shown in Fig. 8. Finally we obtain for the quality factor:

$$Q_{TBP} = \frac{f_{res}}{B} \leq 40.54. \tag{14}$$

Due to the fact that the ohmic losses in loop antennas are typically low, even in the HF-band, the resulting Q-factor of standard loop antennas for NFC devices is well above the obtained limits. Hence, it is necessary to reduce the antenna's quality factor by means of an additional damping resistance in parallel to the loop antenna. With this resistance value in the parameter space of the numerical optimization process we are also able to implicitly take into account the signal shape related requirements in the synthesis of the loop geometry and the matching circuit in frequency domain simulations.

IV. Optimization Problems

In the following we discuss into detail the actual problem under investigation. Starting from the definition of the objectives and the construction of the cost function, the used PEEC model as well as a surrogate model is introduced.

A. Construction of the cost function and applied optimization strategies

As already addressed, the problem under investigation is a multi-objective problem. Beside the two discussed contending objectives power and Q-factor also the NFC-IC specific maximum current which the IC is able to provide has to be taken into account. In addition to these objectives (I_{IC}, Q-factor, H_{min} L_1, L_3, L_6, H_{max} L_1, L_3, L_6) we decided to consider the resulting number of turns, since from the perspective of mass production and costs this is also a very important objective.
It is known from the literature (e.g. [24]) that a so called multi- or many-objective optimization problem defined as:

$$\min_x \left(f_1(x), f_2(x), \dots, f_k(x)\right) \quad subject\ to\ x \in X, \tag{15}$$

with a possibly very heterogeneous parameter space X (in our case electric parameters of lumped components and geometrical parameters of the antenna structure), and a set of typically non-convex objective functions $f_k(x)$ leads to a non-linear constrained problem.
Quite often it can happen that two or more objectives cannot be improved at the same time within multi-objective problems. For instance it is not possible for loop antenna problems to increase the system's quality factor and the system bandwidth at the same time. This means that it is possible that no general optimal solution to this problem can be found. Instead, it is said that some Pareto-optimal solutions exist [24]. The determination of those Pareto-optimal solutions is possible by applying appropriate optimization strategies like the well-known NSGA-II algorithm [25]. With the obtained solutions, the so called Pareto-front can be constructed which consists of the non-dominated solutions. Those non-dominated solutions are all feasible and it is the development engineer's responsibility to evaluate them and make a proper choice for the design. The computation of the Pareto-front can be time consuming and in case of more than three objectives the visualization is problematic which can be obstructive for the engineer. The second possibility to treat such multi- or many-objective problems is to create a single scalar objective function by merging the various separate objective functions e.g. by minimizing the weighted sum of the objectives.
It has to be noted that the various objective functions of the optimization problem can deliver results in quite different ranges of values. E.g. the power levels are in the mW region, whereas the Q-factor can be up to 40 as elaborated in section III. To overcome this problem, a special weighting of the specific objectives is necessary. A simple method for this scaling or weighting is given by means of so called membership functions $\mu_n(f_m(x))$ [26] which map the objectives to a scalar value, the so called quality contribution. Finally, it is assumed that by minimizing the scalar objective function given by:

$$\min_x \left(\mu_1(f_1(x)) + \mu_2(f_2(x)) + \dots + \mu_k(f_k(x))\right) \quad subject\ to\ x \in X, \tag{16}$$

a single Pareto-optimal solution can be obtained. This type of optimization is also called optimization in the multi-objective sense.
Two cases of membership functions have been investigated into more details.
In case of so called linear membership functions [26] an interval region is defined where the function decreases linearly to zero as shown in Fig. 9. For objectives with a confidence interval which is bounded from both sides (like the Q-factor) also two sided linear membership functions are defined.

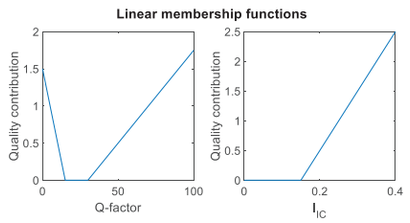

Fig. 9. Linear membership functions for Q-factor and I_{IC}.

The second possibility is to use sigmoidal fuzzy functions [26] where especially the transition zones are smoothed which has been shown to be advantageous for the convergence behavior [27]. A comparison of the two approaches is presented in section V.

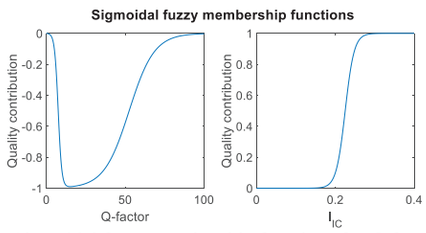

Fig. 10. Sigmoidal fuzzy membership functions for Q-factor and I_{IC}.

Finally three objective functions were elaborated in more details:
In the first case only linear membership functions μ_{lin} have been used for the scaling of the objective. The optimization problem reads as follows:

$$\min_{\mathbf{p}} \Bigg(\mu_{lin1}(N_{turn}(\mathbf{p})) + \mu_{lin2}(Q_{Ant}(\mathbf{p})) + \mu_{lin3}(I_{IC}(\mathbf{p})) + \sum_{i=1,3,6} \mu_{lin_{min}i}\left(min_{all\ pos}\left(H_{min\ L_i}(\mathbf{p})\right)\right) + \sum_{i=1,3,6} \mu_{lin_{max}i}\left(max_{all\ pos}\left(H_{max\ L_i}(\mathbf{p})\right)\right)\Bigg). \tag{17}$$

The first summand describing the number of turns is straight forward whereas the determination of the Q-factor implies an adaptive frequency sweep to find the resonance frequency and the 3dB corner points to compute the bandwidth B and

consequently the Q-factor by means of $Q = f_{res}/B$. In the third summand the maximum current of all positions in the operating volume is used. For the H_{min}-test a similar approach is used. Here the lowest power level for all test positions is used to compute the quality contribution. For the H_{max}-test the highest power level for all positions is used.

In the second test case the same objective function is used to compute the quality, but instead of μ_{lin} sigmoidal fuzzy functions μ_{sig} are used.

In the *third* test case not only the minimum and maximum values for the H_{min}- and H_{max}-tests have been used, but instead the information of the H_{min} and H_{max} values in all test points with position index p in the operating volume have been used to compute the quality of the individuals. The objective function for this optimization problem reads as follows:

$$\min_{\mathbf{p}} \Bigg(\mu_{sig1}\big(N_{turn}(\mathbf{p})\big) + \mu_{sig2}\big(Q_{Ant}(\mathbf{p})\big) + \mu_{sig3}\big(I_{IC}(\mathbf{p})\big) + \sum_{i=1,3,6} \sum_{p=1}^{14} \mu_{sigi}\Big(H_{minL_{ip}}(\mathbf{p})\Big) + \sum_{i=1,3,6} \sum_{p=1}^{14} \mu_{sigi}\Big(H_{maxL_{ip}}(\mathbf{p})\Big) \Bigg). \quad (18)$$

It has been shown (e.g. in [28]) that stochastic optimization strategies are a good choice for problems with very little knowledge about the behavior of the objective function because they tend to find the region of the global minimum with a very high probability. Due to the fact that for the present problem a rather large number of resonances and consequently a multi modal behavior is expected stochastic optimization strategies have been chosen. A very promising representative for this group of optimization strategies is for example the Differential Evolution (DE) strategy which has been applied to the NFC problem in the form $DE/best/1$ which means that the construction of the donor $\mathbf{v}_i$ in the mutation step is given by:

$$\mathbf{v}_i = \mathbf{x}_{best} + F(\mathbf{x}_{r2} - \mathbf{x}_{r3}). \quad (19)$$

Where $\mathbf{x}_{best}$ is the parameter vector of the current optimal individual, $F \in [0,1]$ is the mutation factor and $\mathbf{x}_{ri}$ are the parameter vectors for two mutually exclusive randomly selected individuals form the current population.

A detailed elaboration of this strategy would go far beyond the scope of this work. Hence, it should be referred to the corresponding literature e.g. [29].

To test whether the obtained solutions belong to the non-dominated Pareto-optimal solutions an optimization based on the NSGA II algorithm has been performed. Due to high computational effort this has been done only for the test problem two with the sigmoidal fuzzy functions.

All simulation results are summarized in section V, where also a comparison with the results obtained from a RBF model is presented.

B. PEEC and surrogate model of the NFC device under test

- PEEC model:

In Fig. 11 the principle sketch of our optimization problem is shown. The NFC device which shall be synthesized consists of a loop antenna which in the present problem is limited to roughly the size of a class 1 loop antenna, a matching circuit and the connected NFC-IC. To enable a rigorous synthesis of the loop geometry a parameterized loop model has been developed. The shape of the loop antenna is defined with the parameters $A_{coil}, k_x, curv$ and A_f. The parameter k_x is defined by the aspect ratio of the two lengths a and b shown in Fig. 12. The parameter $curv$ gives a fractional amount of the total coil area A_{coil} which is then used to compute the radius of the quarter circles shown in Fig. 12 and A_f determines implicitly the maximum number of turn by defining an area where no conductive parts of the loop structure are allowed. With this kind of model we are able to synthesize loops from one turn and complete circular shape to rectangular shaped loops with a certain number of turns depending especially on the parameter A_f (see Fig. 13). It should be noted that the distance between the turns as well as the cross section of the turns was kept constant during the optimization process. The initial box bounds for the geometrical parameters of the loop antenna are summarized in Table II.

TABLE II. PARAMETER SPACE FOR THE LOOP GEOMETRY AND THE MATCHING CIRCUIT.

Parameter	*min*	*max*
k_x	0.1	0.9
$curv$	0.1	0.9
A_f	0.85	0.95
C_r	10^{-12} in F	10^{-8} in F
C_m	10^{-12} in F	10^{-8} in F
R_d	10^{0} in Ω	10^{4} in Ω

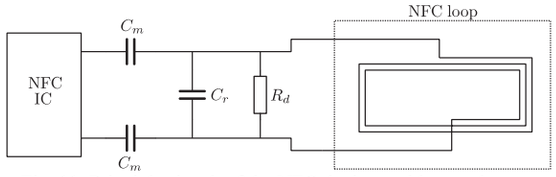

Fig. 11. Principle sketch of the NFC device problem under test.

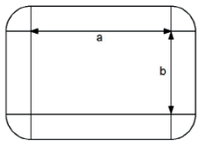

Fig. 12. Definition of the geometry parameter k_x in terms of a and b.

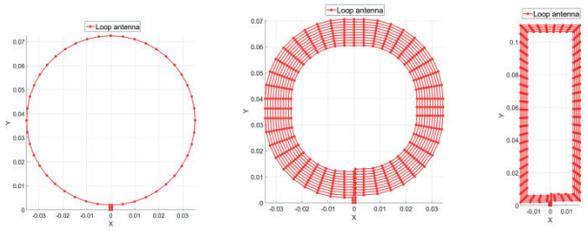

Fig. 13. Various loop antenna geometries with PEEC stick element discretization.

For the matching circuit a commonly used reactive circuit consisting of three capacitors [30] was chosen as shown in Fig. 11, too. The reason for limiting the reactive elements to capacitors is beside physical size issues the fact that in general inductors are much more expensive than capacitors. Especially from the perspective of the mass market this is a very important point. It should be noted, that a more rigorous approach for the matching circuit would be to model the circuit as a passive two port network but again this would probably result in a circuit consisting of inductors which

should be omitted. The parameters of the matching circuit with their initial box bounds are given in Table II, too.
The antenna structure of the loop antenna is now discretized by means of the 1D stick elements as introduced in section II and the resulting system of equations (see (9)) extended with the lumped components of the matching circuit finally results to the form given in (10). In Fig. 13 plots of stick-element discretized antennas are shown. The circles in Fig. 13 represent the nodes where the various sticks are connected. Due to the fact that the shape of the antenna is completely arbitrary a strategy was developed which controls the lengths of the sticks dynamically. A comprehensive discussion of this strategy goes again far beyond the scope of this work and shall therefore not be elaborated in more details here.

- Surrogate model:

In [31] it is stated that in those cases where roughly the number of available samples is greater than 500 and the number of design variables is less than 20 it is advised to apply radial basis function (RBF) interpolation for creating surrogate models. Based on this rule of thumb RBF were chosen to model the objectives. Further benefits are the fast fitting time and the fast evaluation of the models because of their simple structure.
RBF models with different basis functions (*linear*, *cubic*, *thin plate spline*, *multi-quadric* and *inverse multi-quadric* [32]) were tested by performing 5-fold cross validation [33] to get a better estimate of the model error. The best for the investigated problem proved to be the multi-quadric basis for which the sigma hyper parameter was also determined by means of 5-fold cross validation. The sigma hyper parameter was selected from 20 candidates in a logarithmic range of [0.001, 100]. Due to the fact that for the present problem 9 objectives are defined (Q-factor, IC current, number of turns and the six power requirements) 9 surrogate models were constructed, one for each of the objectives. The resulting sigma hyper parameters for the objectives are listed in Table III.

TABLE III. HYPER PARAMETERS FOR THE OBJECTIVES.

Objective	σ	Objective	σ
N_{turns}	0.0062	$H_{min}\ L_6$	0.0062
Q-factor	0.0018	$H_{max}\ L_1$	0.011
I_{IC}	0.038	$H_{max}\ L_3$	0.0034
$H_{min}\ L_1$	0.021	$H_{max}\ L_6$	0.021
$H_{min}\ L_3$	0.011		

In Fig. 14 to Fig. 15 a comparison of the results obtained from the PEEC model and the surrogate models is given. In total 500 samples have been used to verify the accuracy of the trained surrogate models (4500 samples have been used for training). To enable a comparison the obtained objective values have been sorted according to their value. As can be seen from Fig 14 (a) the Q-factor objective is the most challenging objective for the RBF surrogate model. The reason for this behavior can be explained by the multimodal landscape of the objective due to resonance effects. The other objectives shown in Fig. 14 (b) and Fig. 15 (a) and (b) are on average approximated very well.

C. Parameter investigations

To determine the influences of geometrical and electrical parameters on the objectives, in advance to the optimization process a variable screening was performed.

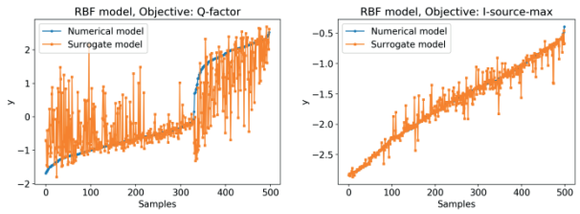

(a) (b)

Fig. 14. Comparison of the objective values obtained from the RBF model and the PEEC model for 500 samples. (a) for the Q-factor (b) for the IC current I_{IC}.

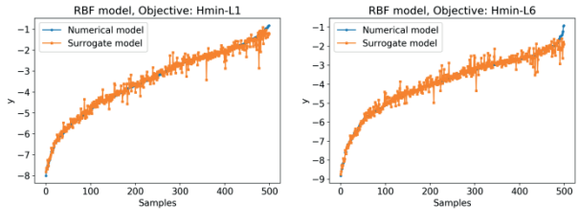

(a) (b)

Fig. 15. Comparison of the objective values obtained from the RBF model and the PEEC model for 500 samples. (a) for the $H_{min}\ L_1$-test (b) for the $H_{min}\ L_6$-test.

In the following a short summary of the applied technique is presented. The method proposed in [34] calculates the mean and standard deviation values of the so called *elementary effects* for each input variable to give information about the role of this variable in the objective function. A high mean value indicating a variable with an important influence on the objective across the whole design space and a high standard deviation value indicating a variable involved in interactions with other variables and maybe in terms in which the objective function is nonlinear. With $D \in \mathbb{R}^k$ being the design space and restricted to a k-dimensional, p-level full factorial grid, where p denotes the number of levels into which the variable range is divided up. That means that $x_i \in D$ is equivalent to $x_i \in \left\{0, \frac{1}{p-1}, \frac{2}{p-1}, \dots, 1\right\}$ for $i = 1, \dots, k$ and $\boldsymbol{x} = [x_1, x_2, \dots, x_k]$. The elementary effect $d_{j,i}(\boldsymbol{x})$ of x_i for the objective y_j, is given by:

$$d_{j,i}(\boldsymbol{x}) = \frac{y_j(x_1, x_2, \dots, x_i + \Delta, \dots, x_k) - y_j(\boldsymbol{x})}{\Delta}. \quad (20)$$

The value for Δ is calculated by $\Delta = \frac{\xi}{p-1}$, where $\xi \in \mathbb{N}^*$ is the elementary effect step length. Now using the elementary effects $d_i(\boldsymbol{x})$ a matrix $\boldsymbol{F}$ is constructed with dimensions $k \times r$, where r is the number of elementary effects recorded for each of the k variables. For example, the i'th row of $\boldsymbol{F}$ contains r elementary effects of variable x_i. A sampling plan $\boldsymbol{B_i^*}$ is generated which employs the presented strategy of extracting one elementary effect for each variable. This sampling plan can be generated by the following equation:

$$\boldsymbol{B}^* = \left(\boldsymbol{1}_{k+1,1}\boldsymbol{x}^* + \frac{\Delta}{2}\left[\left(2\boldsymbol{B} - \boldsymbol{1}_{k+1,k}\right)\boldsymbol{D}^* + \boldsymbol{1}_{k+1,k}\right]\right)\boldsymbol{P}^*. \quad (21)$$

Where $\boldsymbol{1}_{k+1,1}$ is a $(k+1) \times 1$ vector of 1's, $\boldsymbol{1}_{k+1,k}$ is a $(k+1) \times k$ matrix of 1's, $\boldsymbol{D}^*$ is a $k \times k$ diagonal matrix, in which the diagonal elements are 1 or -1 with equal probability, $\boldsymbol{x}^*$ is a $1 \times k$ vector of values randomly selected from $\left\{0, \frac{1}{p-1}, \frac{2}{p-1}, \dots, 1\right\}$ with equal probability, $\boldsymbol{B}$ is a $(k+1) \times k$ matrix consisting of 0's and 1's in such a way that columns i and $i+1$ differ only in the i'th row and $\boldsymbol{P}^*$ is a $k \times k$ random permutation matrix where each column has one element equal to 1 and all others equal to 0 and no two columns have a 1 in the same row. To calculate the before mentioned r elementary effects, r matrices $\boldsymbol{B}^*$ are generated and stacked to form $\boldsymbol{X}$**:**

$$\boldsymbol{X} = \begin{bmatrix} \boldsymbol{B}_1^* \\ \vdots \\ \boldsymbol{B}_r^* \end{bmatrix}. \quad (22)$$

Performing the presented approach for our optimization problem with $r = 100$, $p = 200$ and $\xi = 1$ a $r(k+1) \times k = 720 \times 6$ preliminary sampling plan was generated and the objectives sampled.

The mean values in Fig. 16 and Fig. 17 provides information about the influence of the specific parameter on the objective, whereas the standard deviation provides additional information of the specific parameter in combination with other parameters and possible non-linear terms as already pointed out. This means the higher the mean value and the standard deviation of a specific parameter is, the higher the parameter influences the objective under investigation. For instance it is obvious from Fig. 16 (a) that the geometrical parameters A_f and k_x have a strong influence on the N_{turns} objective. The Q-factor objective instead is strongly influenced by the matching capacitance C_m and the damping resistance R_d as shown in Fig. 16 (b). In Fig. 17 (a) the influences of the parameters on the I_{IC} objective and in Fig. 17 (b) on the H_{min} L_6 objective are shown. Again the electric parameters show high mean and standard deviation values.

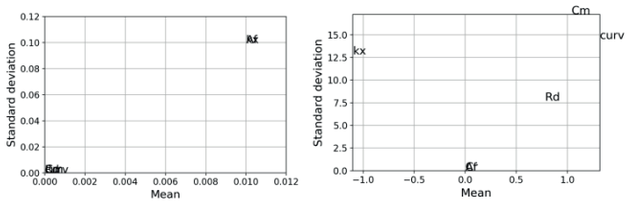

(a) (b)

Fig. 16. Mean value and standard deviation of the parameters obtained from the sampling plans for the objectives for (a) N_{turns} and (b) Q-factor.

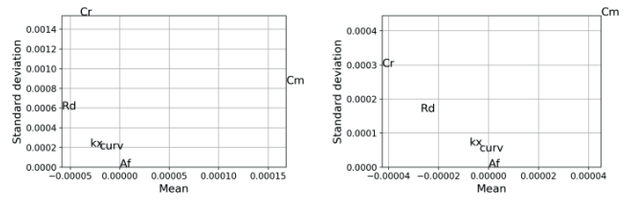

(a) (b)

Fig. 17. Mean value and standard deviation of the parameters obtained from the sampling plans for the objectives for (a) I_{IC} max (b) H_{min} L_6.

It is possible to use the generated samples with a specified region of interest of the objective values and plot a distribution of the design variables in the region of interest and use these plots to reduce the variable range and allow a finer sampling of the objective region of interest.

In the following a summary and comparison of the most interesting findings is presented. The results obtained are based on the preceding variable screening.

As one can see from Fig. 18 (a), in the case of the Q-factor objective the matching capacitor and damping resistor ranges can be almost halved in both cases, a similar situation is observed with the resonance capacitor in the case of the H_{min} L_6 objective in Fig. 18 (b). Looking at these two objectives and the distribution of the matching capacitor values it is evident that a compromise has to be made as the distribution in one case flattens out where it in the other case goes up and vice versa. The observed behavior can be explained in a physical manner: the power requirement objective and the Q-factor objective are two contending objectives as already

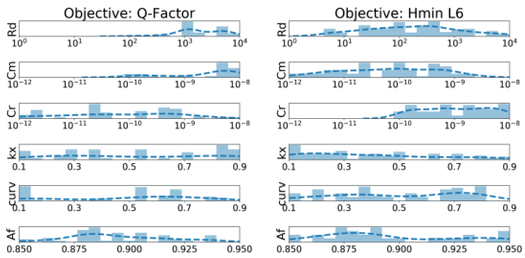

(a) (b)

Fig. 18. Distribution of the design variables in the initial box bounded regions for the objectives (a) Q-factor and (b) H_{min} $L6$-test.

pointed out in section III. In Table IV the new box bounds for the electrical parameters based on the variable screening are summarized. As can be seen from Fig. 18 (a) and (b) a restriction for the geometrical parameters based on the screening is not advisable.

TABLE IV. PARAMETER SPACE OF THE ELECTRIC CIRCUIT PARAMETERS.

	R_d in Ω	C_r in F	C_m in F
Original bounds	10^{0}-10^{4}	10^{-12}-10^{-8}	10^{-12}-10^{-8}
Reduced bounds	$10^{1.6}$-10^{4}	$10^{-10.4}$-10^{-8}	$10^{-10.8}$-10^{-8}

V. SIMULATION RESULTS

It became apparent that two objectives are rather hard two fulfill. Especially for the Q-factor and the H_{min}-test for the Listener 6 device convergence problems can be observed. This behavior is from the technical point of view not surprising since - as already pointed out - the power transfer and the Q-factor are two contending objectives. Especially for the rather small loop antenna of the Listener 6 device the compliance to the power requirement is becoming cumbersome. To be able to provide valid conclusions the optimization processes have been executed 30 times for the DE optimized problems. For those problems a swarm size of 30 individuals and a maximum iteration number of 250 iterations were used.

In the plots from Fig. 19. to Fig. 23 the convergence behaviors of selected objectives for the test problem *one* defined by (16) are given. As can be seen from Fig. 19 also for high iteration numbers still Q-factor values outside the confidence region are obtained. In Fig. 23 the mean difference between the obtained global best solution per run and the minimum power for the H_{min} L_6-test is plotted. As can be seen the H_{min} L_6-test shows a rather slow convergence and seems to be very challenging for this test case.

In Fig. 24 to Fig. 27 selected combinations of the best obtained parameters are plotted. Two very interesting observations should be discussed into more details. In Fig. 24 (a) the resonance and matching capacitances C_r and C_m are plotted. As can be seen two highly populated clusters are obtained.

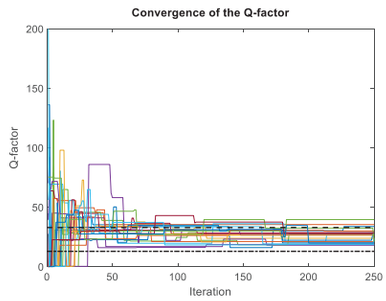

Fig. 19. Convergence behavior of the Q-factor. The black dashed and dash-dotted lines give the confidence interval of the objective.

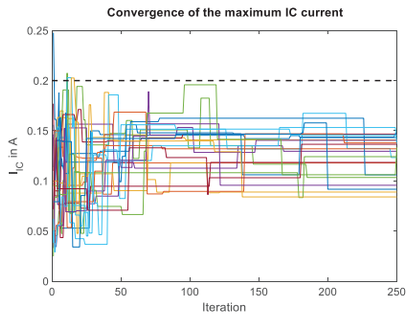

Fig. 20. Convergence behavior of the IC current I_{IC}. The black dashed line gives the maximum current according to the datasheet.

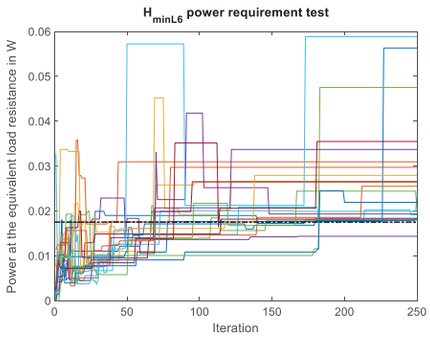

Fig. 21. Convergence behavior of the H_{min} L_6-test. The black dash-dotted line gives the minimum power for standard compliance.

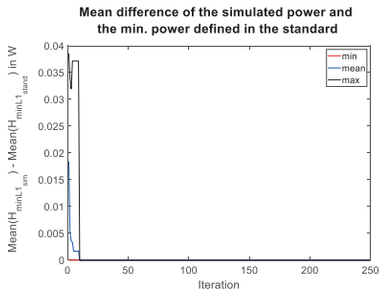

Fig. 22. Convergence behavior of the H_{min} L_1-test.

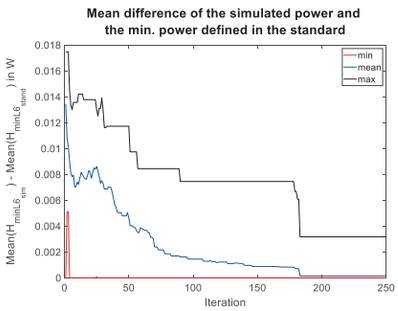

Fig. 23. Convergence behavior of the H_{min} L_6-test.

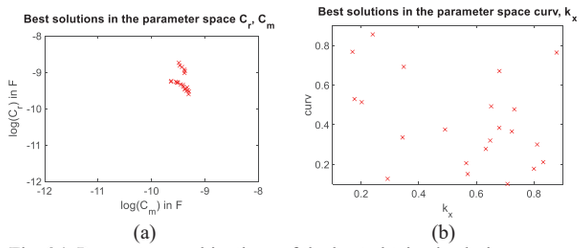

(a) (b)

Fig. 24. Parameter combinations of the best obtained solution per run. (a) C_r, C_m and (b) *curv*, k_x.

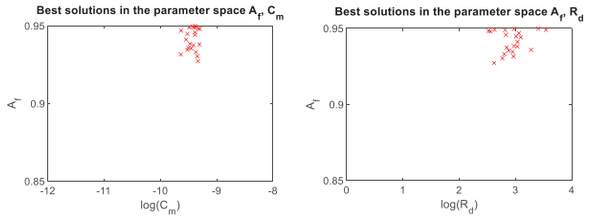

(a) (b)

Fig. 25. Parameter combinations of the best obtained solution per run. (a) A_f, C_m and (b) A_f, R_d.

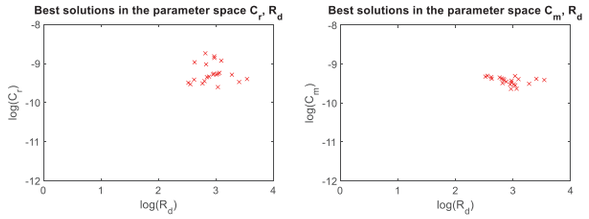

(a) (b)

Fig. 26. Parameter combinations of the best obtained solution per run. (a) C_r, R_d and (b) C_m, R_d.

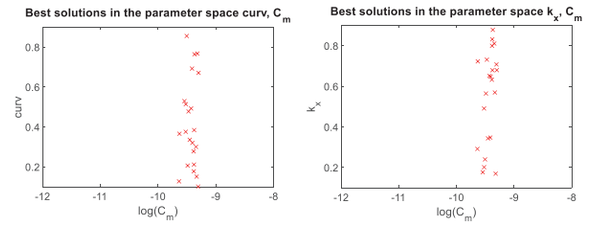

(a) (b)

Fig. 27. Parameter combinations of the best obtained solution per run. (a) *curv*, C_m and (b) k_x, C_m.

The reason for this behavior can be explained by the rather sharp resonances in the frequency domain. On the other hand the parameters $curv$ and k_x are distributed over the whole parameter space as shown in Fig. 24 (b), hence it seems that for the defined cost function the shape of the loop plays a subordinate role. The concentration of the best solutions for the parameter combinations A_f, C_m and A_f, R_d in Fig. 25 (a) and (b) can be explained by the objective for the number of turns, again by the resonance behavior and the matching between the IC and the antenna. The concentration of the parameters in Fig. 26 (a) and (b) to local clusters points out that the matching and Q-factor reduction is vital. Fig. 27 (a) and (b) show again that the shape of the antenna plays a subordinate role for this problem.

Selected convergence plot for the test problem *two* with sigmoidal fuzzy functions are shown in the Fig. 28 to Fig. 29. The Q-factor objective in Fig. 28 shows a comparable convergence as for the test problem *one*. But as can be seen from Fig. 29 the mean difference in the power levels for the H_{min} L_6-test shows on average a better convergence behavior than for the test problem one. Hence, it can be concluded that the smoothening in the transition zone by the sigmodal fuzzy functions is appropriate.

In the plots shown in Fig. 30 to Fig. 31 again some selected parameter combinations of the best obtained solutions per run are show. The obtained distributions are practically equivalent to the parameter plots for the test problem *one*.

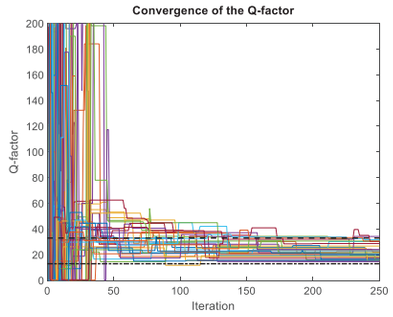

Fig. 28. Convergence behavior of the *Q*-factor. The black dashed and dash-dotted lines give the confidence interval of the objective.

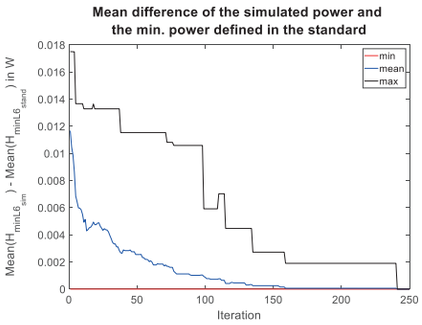

Fig. 29. Convergence behavior of the $H_{min}\,L_6$-test.

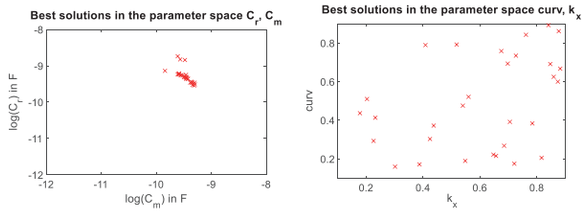

(a) (b)

Fig. 30. Parameter combinations of the best obtained solution per run. (a) C_r, C_m and (b) *curv*, k_x.

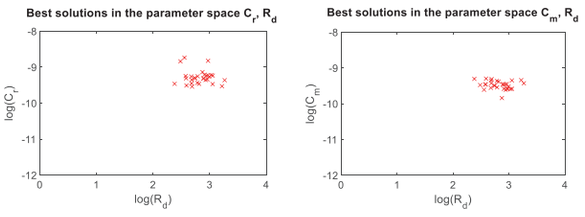

(a) (b)

Fig. 31. Parameter combinations of the best obtained solution per run. (a) C_r, R_d and (b) C_m, R_d.

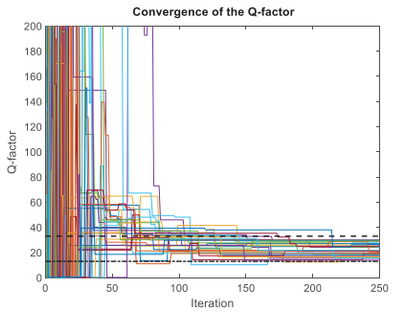

Fig. 32. Convergence behavior of the *Q*-factor. The red dashed and dash-dotted lines give the confidence interval of the objective.

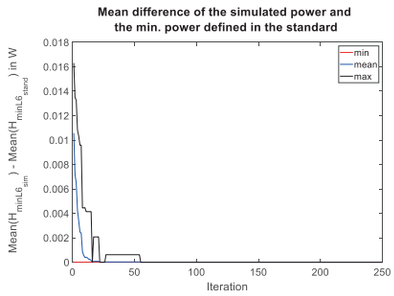

Fig. 33. Convergence behavior of the $H_{min}\,L_6$-test.

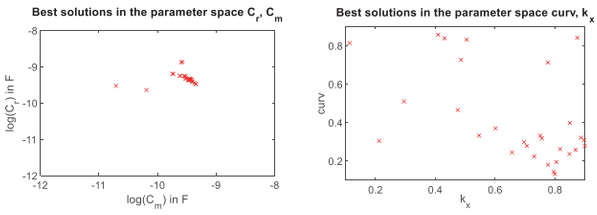

(a) (b)

Fig. 34. Parameter combinations of the best obtained solution per run. (a) C_r, C_m and (b) *curv*, k_x.

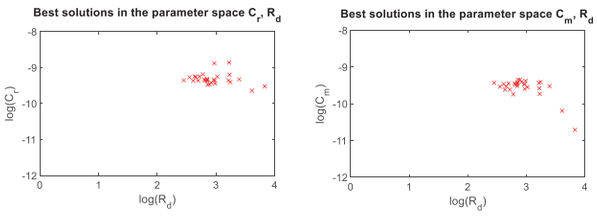

(a) (b)

Fig. 35. Parameter combinations of the best obtained solution per run. (a) C_r, R_d and (b) C_m, R_d.

The simulation results for the test problem *three* are shown in Fig. 32 to Fig. 35. Again only a selection is shown. Using not just only the information of the worst cases in the power test but the power at each position in the operating volume dramatically increases the performance of the convergence behavior also for the most challenging $H_{min}\,L_6$-test as shown in Fig. 33. and in Fig. 36 where a comparison of the three test problems is plotted. Also for test problem *three* the electrical parameters tend to cluster to rather small domains in the parameter space (e.g. see Fig. 34 (a)). On the other hand the geometrical parameters are distributed widely in the parameter space and again play a subordinate role.

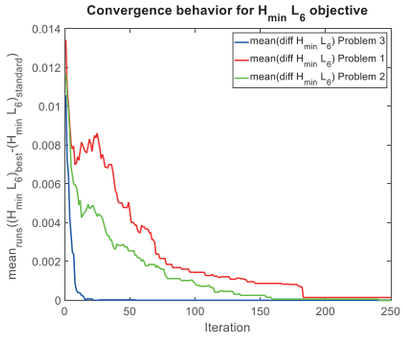

Fig. 36. Convergence behavior of the $H_{min}\,L_6$-test. Comparison of the three test problems

A comparison between the obtained results from the test problem *two* with results obtained by applying the NSGA II algorithm is given in the Fig. 37 to Fig. 39. It should be noted that for the NSGA II optimization the original bounds given in Table IV have been used. Also here only a selection of the

data set can be presented. In Fig. 37 to Fig. 38 the contribution to the overall quality for specific combinations of objectives is presented. As can be seen from Fig. 37 (a) and (b) the DE optimized solutions are all very close to the utopia point for these selections. The NSGA algorithm was not able to detect all of these solutions. On the other hand, as shown in Fig. 38 (a) and (b), also the NSGA algorithm was able to detect most of the solutions which were obtained by the DE optimizer for these specific combinations. In Fig. 39 and Fig. 40 a selection of the best solutions in selected parameter spaces is presented. Especially Fig. 39 (a) shows a very good agreement between NSGA and DE for the values of C_r and C_m. On the other hand as can be seen from Fig. 40 (a) and (b) the DE obtained solutions are not in the same solution space as obtained by the NSGA algorithm. Since the value of R_d also dominates the Q-factor of the antenna the quality contributions shown in Fig. 37 (a) and (b) can be explained by this parameter mismatch. It should be noted at this point that for the DE optimization up to 7500 function calls per run have been evaluated, whereas for the NSGA II optimization more than 20.000 function evaluations have been executed.

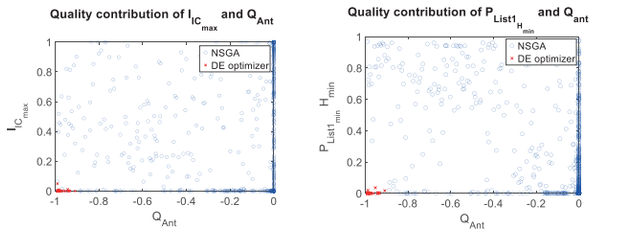

(a) (b)

Fig. 37. Pareto-front subset of the best obtained solution per run. (a) I_{IC}, Q_{Ant} and (b) $H_{min}L_1$, Q_{Ant}.

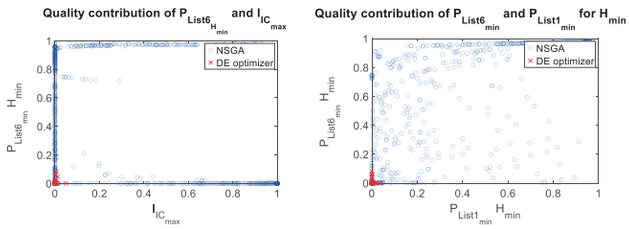

(a) (b)

Fig. 38. Pareto-front subset of the best obtained solution per run. (a) $H_{min}L_6$, I_{IC} and (b) $H_{min}L_6$, $H_{min}L_1$.

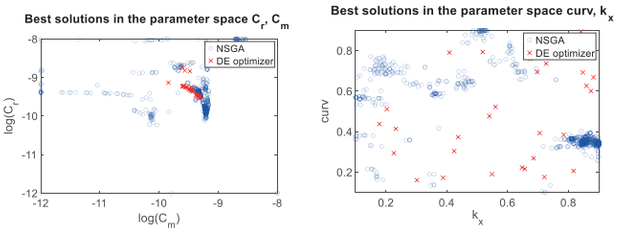

(a) (b)

Fig. 39. Parameter combinations of the best obtained solution per run. (a) C_r, C_m and (b) *curv*, k_x.

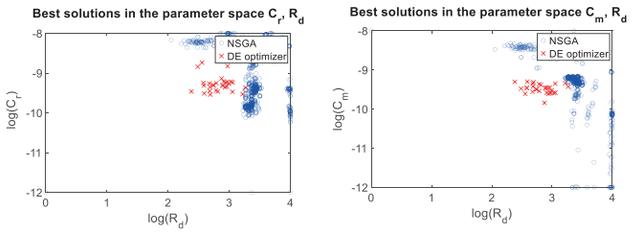

(a) (b)

Fig. 40. Parameter combinations of the best obtained solution per run. (a) C_r, R_d and (b) C_m, R_d.

Finally also a comparison between the PEEC based optimization and the surrogate model based optimization applying a RBF based approach is presented in Fig. 41.

The test problem *two* was used here for both optimization processes. As can be seen from Fig. 41 (a) a very good agreement for the electrical parameters C_r, C_m for the RBF model is given. Already the parameter screening has shown that especially the electrical parameters of the matching circuit show a much higher impact on the system parameters like the Q-factor or the H_{min}-test. Hence, the obtained good agreement in the C_r, C_m-parameter space is of much higher importance than a possible mismatch in the parameter space of the geometrical parameters.

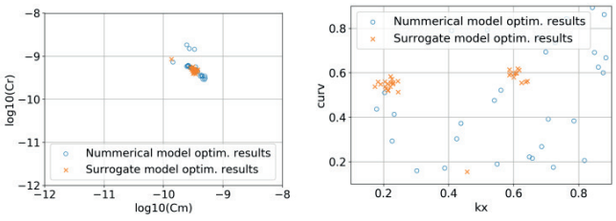

(a) (b)

Fig. 41. Parameter combinations of the best obtained solution per run. (a) C_r, C_m and (b) *curv*, k_x.

V. Conclusion and Outlook

In the present work the numerically assisted synthesis of NFC antennas has been discussed. A PEEC model as well as a RBF based model used in the numerical optimization process have been introduced and discussed. Linear and sigmoidal membership functions have been applied to construct single scalar objective functions for the optimization of the NFC antenna geometry and the electrical parameters of the needed matching circuit. In advance to the numerical optimization a variable screening of the design variables has been carried out to reduce the parameter space and consequently enhance the optimization process. DE and NSGA algorithms were finally applied beside the RBF model to synthesize the loop geometry and the electric circuit parameters of the matching circuit. All models have shown that the initially anticipated conflicting behavior of the objectives antenna quality factor and power requirements is observable. The obtained parameter space for the most affecting design variables C_r, C_m, and R_d for these objectives could be located by all applied optimization strategies. Whereby the computational costs of the RBF model are significantly smaller than those of the DE algorithm.

The implicit consideration of the modulation scheme in the optimization process in terms of the Q-factor is noticed as problematic. Therefore, it is planned to take into account the non-linear behavior of the Listener devices in the optimization process in terms of steady state solutions of the time dependent test signals. First promising numerical experiments have shown that also time domain simulations can be incorporated in the synthesis process in a hybrid manner.

VI. References

[1] ISO/IEC 14443: Identification cards – Contactless integrated circuit cards – Proximity cards – Part 1, 2, 3 and 4, ISO, Geneva, Switzerland, 2018.

[2] ISO/IEC 15693: Identification cards – Contactless integrated circuit cards – Vicinity cards – Part 1, 2 and 3, ISO, Geneva, Switzerland, 2019.

[3] JIS X 6319-4: Specification of implementation for integrated circuit(s) cards - Part 4: High speed proximity cards, Japanese Standards Association, 2016.
[4] NFC Forum: NFC Analog Technical Specification, Version 2.1, August 2018.
[5] Gebhart, M. and Bauernfeind, T., "Loop antennas for Near Field Communication." *Compendium on Electromagnetic Analysis: From Electrostatics to Photonics: Fundamentals and Applications for Physicists and Engineers*. World Scientific, 2018, pp. 245-299.
[6] Minihold, R., "*Near Field Communication (NFC) Technology and Measurements*", Rohde & Schwarz White Paper, 2011.
[7] Wobak, M., Gebhart, M., and Muehlmann. U., "Physical limits of batteryless HF RFID transponders defined by system properties", *2012 IEEE International Conference on RFID-Technologies and Applications (RFID-TA)*. IEEE, 2012, pp. 142-147.
[8] Gebhart, M., "Analytic-numeric considerations for contactless reader modulation", *2015 13th International Conference on Telecommunications (ConTEL).* IEEE, 2015, pp. 1-8.
[9] Gebhart, M. and Szoncso, R., "Optimizing design of smaller antennas for proximity transponders", *2010 Second International Workshop on Near Field Communication*. IEEE, 2010, pp. 77-82.
[10] Gebhart, M., et al. "Design of 13.56 MHz smartcard stickers with ferrite for payment and authentication", *2011 Third International Workshop on Near Field Communication*. IEEE, 2011, pp. 59-64.
[11] Schober, A., Ciacci, M., and Gebhart, M., "An NFC air interface coupling model for contactless system performance estimation", *Proceedings of the 12th International Conference on Telecommunications*. IEEE, 2013, pp. 243-250.
[12] Ruehli, A. E., "Equivalent circuit models for three-dimensional multiconductor systems", *IEEE Transactions on Microwave theory and techniques,* vol. 22(3), 1974, pp. 216-221.
[13] Orfanidis, S.J., *Electromagnetic Waves and Antennas.* Piscataway, NJ, USA: Sophocles J. Orfanidis, Aug. 2016. [Online]. Available: http://www.ece.rutgers.edu/~orfanidi/ewa
[14] Torchio, R., Bettini, P., and Alotto, P., "PEEC-Based analysis of complex fusion magnets during fast Voltage transients with H-matrix compression", *IEEE Transactions on Magnetics*, vol. 53(6), 2017, pp. 1-4.
[15] Voltolina, D., Bettini, P., Alotto, P., Moro, F., and Torchio, R., "High-Performance PEEC analysis of electro-magnetic scatterers", *IEEE Transactions on Magnetics*, vol. 55(6), 2019, pp. 1–4.
[16] Ardon, V., et al. "EMC modeling of an industrial variable speed drive with an adapted PEEC method", *IEEE Transactions on Magnetics*, vol. 46(8), 2010, pp. 2892–2898.
[17] Torchio, R., *Extending the unstructured PEEC method to magnetic, transient, and stochastic electromagnetic problems*, Ph.D. dissertation, Università degli Studi di Padova and Universitè Grenoble Alpes, 2019.
[18] ETSI EN 300 330-1 and -2, "Electromagnetic compatibility and Radio spectrum Matters (ERM); Short Range Devices (SRD); Radio equipment in the frequency range 9 kHz to 25 MHz and inductive loop systems in the frequency range 9 kHz to 30 MHz", 2015.
[19] Bauernfeind, T., et al. "Multi-objective synthesis of NFC-transponder systems based on PEEC method", *IEEE Transactions on Magnetics,* vol. 54(3), 2017, pp. 1-4.
[20] ISO/IEC10373-6: Cards and security devices for personal identification - Test methods - Part 6: Contactless proximity objects. ISO, Geneva, Switzerland, 2020.
[21] Bauernfeind, T., et al. "PEEC-based multi-objective synthesis of NFC antennas in the presence of conductive structures", *2018 International Applied Computational Electromagnetics Society Symposium (ACES)*. IEEE, 2018, pp. 1-2.
[22] Gebhart, M., et al. "Automatic analysis of 13.56 MHz reader command modulation pulses", *Eurasip RFID Workshop*. 2008.
[23] Girod B., Rabenstein R., Stenger A., *Einführung in die Systemtheorie: Signale und Systeme in der Elektrotechnik und Informationstechnik*, B. G. Teubner Stuttgart,·Leipzig, Wiesbaden, 2003.
[24] Di Barba, P., *Multiobjective Shape Design in Electricity and Magnetism.* Lecture Notes in Electrical Engineering, vol. 47, Springer, 2009.
[25] Deb, K., Pratap, A., Agarwal, S., and Meyarivan, T.,"A fast and elitist multiobjective genetic algorithm: NSGA-II", *IEEE Transactions on Evolutionary Computation*, vol. 6(2), 2002, pp. 182-197.
[26] Baumgartner, P., et al. "Multi-objective optimization of Yagi–Uda antenna applying enhanced firefly algorithm with adaptive cost function", *IEEE Transactions on Magnetics* , vol. 54(3), 2017, pp. 1-4.
[27] Magele, C., et al. "Self adaptive fuzzy sets in multiobjective optimizations using genetic algorithms", *Applied Computational Electromagnetics Society Journal* , vol 2(12), 1997, p. 26-31.
[28] Alotto, P., et al. "Stochastic algorithms in electromagnetic optimization", *IEEE Transactions on Magnetics*, vol. 34(5), 1998, pp. 3674-3684.
[29] Alotto, P., "A hybrid multiobjective differential evolution method for electromagnetic device optimization", *COMPEL - The international journal for computation and mathematics in electrical and electronic engineering*, vol. 30(6), 2011, pp. 1815-1828.
[30] NXP application note AN11564, "PN7120 antenna design and matching guide", 2016. Available: https://www.nxp.com/docs/en/application-note/AN11564.pdf
[31] Forrester, A., Sobester, A., Keane, A., *Engineering Design via Surrogate Modelling*, Wiley, 2008.
[32] Buhmann, M. D., *Radial basis functions: theory and implementations*, Cambridge University Press, 2003.
[33] Berrar, D., "Cross-validation", *Encyclopedia of Bioinformatics and Computational Biology*, vol. 1, 2019, pp. 542-545.
[34] Morris, M. D., "Factorial sampling plans for preliminary computational experiments", *Technometrics*, vol. 33(2), 1991, pp. 161-174.

AUTHORS NAME AND AFFILIATION

Thomas Bauernfeind, Paul Baumgartner, Eniz Mušeljić
Institute of Fundamentals and Theory in Electrical Engineering, Graz University of Technology, Inffeldgasse 18, 8010 Graz, Austria
+43 316 873 7750, t.bauernfeind@tugraz.at
Riccardo Torchio
Department of Industrial Engineering, University of Padova, Via Gradenigo 6a, 35131 Padova, Italy